INTERFACE FOCUS

rsfs.royalsocietypublishing.org

Review

Cite this article: Rtimi S, Nesic J, Pulgarin C, Sanjines R, Bensimon M, Kiwi J. 2015 Effect of surface pretreatment of TiO_2 films on interfacial processes leading to bacterial inactivation in the dark and under light irradiation. *Interface Focus* **5**: 20140046.
http://dx.doi.org/10.1098/rsfs.2014.0046

One contribution of 15 to a theme issue 'Biological adhesives: from biology to biomimetics'.

Subject Areas:
chemical engineering, environmental science, biomaterials

Keywords:
TiO_2 interface, bacterial inactivation, thin film, transmission electron microscopy, dark disinfection, aggregation

Author for correspondence:
John Kiwi
e-mail: john.kiwi@epfl.ch

Effect of surface pretreatment of TiO_2 films on interfacial processes leading to bacterial inactivation in the dark and under light irradiation

Sami Rtimi[1], Jelena Nesic[1,2], Cesar Pulgarin[1], Rosendo Sanjines[3], Michael Bensimon[4] and John Kiwi[5,†]

[1]Ecole Polytechnique Fédérale de Lausanne, EPFL-SB-ISIC-GPAO, Station 6, 1015 Lausanne, Switzerland
[2]Faculty of Chemistry, University of Belgrade, Studentski trg 12, Belgrade, Serbia
[3]Ecole Polytechnique Fédérale de Lausanne, EPFL-SB-IPMC-LNNME, Bat PH, Station 3, 1015 Lausanne, Switzerland
[4]Ecole Polytechnique Fédérale de Lausanne, EPFL-ENAC-IIEGR-CEL, Bat GC, Station 18, 1015 Lausanne, Switzerland
[5]Ecole Polytechnique Fédérale de Lausanne, EPFL-SB-ISIC-GPAO, Bat Chimie, Station 6, 1015 Lausanne, Switzerland

Evidence is presented for radio-frequency plasma pretreatment enhancing the amount and adhesion of TiO_2 sputtered on polyester (PES) and on polyethylene (PE) films. Pretreatment is necessary to attain a suitable TiO_2 loading leading to an acceptable *Escherichia coli* reduction kinetics in the dark or under light irradiation for PES–TiO_2 and PE–TiO_2 samples. The amount of TiO_2 on the films was monitored by diffuse reflectance spectroscopy and X-ray fluorescence. X-ray electron spectroscopy shows the lack of accumulation of bacterial residues such as C, N and S during bacterial inactivation since they seem to be rapidly destroyed by TiO_2 photocatalysis. Evidence was found for Ti^{4+}/Ti^{3+} redox catalysis occurring on PES–TiO_2 and PE–TiO_2 during the bacterial inactivation process. On PE–TiO_2 surfaces, Fourier transform infrared spectroscopy (ATR-FTIR) provides evidence for a systematic shift of the $n_a(CH_2)$ stretching vibrations preceding bacterial inactivation within 60 min. The discontinuous IR-peak shifts reflect the increase in the C–H inter-bond distance leading to bond scission. The mechanism leading to *E. coli* loss of viability on PES–TiO_2 was investigated in the dark up to complete bacterial inactivation by monitoring the damage in the bacterial outer cell by transmission electron microscopy. After 30 min, the critical step during the *E. coli* inactivation commences for dark disinfection on 0.1–5% wt PES–TiO_2 samples. The interactions between the TiO_2 aggregates and the outer lipopolysaccharide cell wall involve electrostatic effects competing with the van der Waals forces.

1. Introduction

TiO_2 has been reported during the last decade to be able to abate bacteria under solar light irradiation [1–8]. Films to reduce/eliminate bacterial infections are becoming increasingly important to preclude the spread of bacteria resistant to antibiotics leading to hospital-acquired infections (HAIs) [9,10]. TiO_2 films should completely inactivate antibiotic-resistant bacteria over a long lifetime in hospital facilities to prevent the spread of infections among patients while they are undergoing treatment.

The low surface energy of polyester (PES) and other textiles and polymer thin films leads to poor TiO_2 nanoparticle adhesion. For this reason, radio-frequency plasma (RF) and ultraviolet light below 320 nm (UVC) were used to pretreat the PES and generate an increased number of active sites, thus enabling increased TiO_2 adhesion. RF-plasma pretreatment induces binding

[†]All authors contributed equally to this paper.

THE ROYAL SOCIETY PUBLISHING

sites for TiO_2 and concomitantly increases the textile hydrophilicity due to the polarity of the surface groups (e.g. –COOH) [11,12]. The fixation of suitable amounts of TiO_2 on fabrics and polymers makes it possible to drive bacterial inactivation over acceptable time scales.

Colloidal deposition of TiO_2 on textiles, polymers, glass and steel plates is used to prepare self-disinfecting and self-cleaning surfaces with a significant photocatalytic activity. But the colloid or sol–gel preparations can lead to films that are not mechanically stable, that are not reproducible, that present low uniformity and that have little adhesion since they can be wiped off by a cloth or thumb [13]. In this report, we will show that pretreating a textile allows the fixation of TiO_2 nanoparticulate films at temperatures compatible with non-heat-resistant materials.

Section 3 of this report addresses the damage to the bacterial outer cell wall by TiO_2 leading to bacterial inactivation [14]. There have been previous reports of cell wall damage due to TiO_2 photocatalysis in *Pseudomonas aeruginosa* [15,16].

Here, we report recent work in our laboratory on: (i) the enhanced deposition of TiO_2 on PES (PET-TiO_2), pretreated by RF-plasma and UVC, (ii) the use of low-intensity actinic light and sunlight to inactivate bacteria on PES–TiO_2, (iii) the reduction of *Escherichia coli* viability in the dark and under light by TiO_2 on PES and polyethylene (PE) substrates, (iv) the surface properties of the PES, PE, PES–TiO_2 and PE–TiO_2 used in the bacterial disinfection, and finally (v) suggestions for the mechanism of *E. coli* inactivation in the dark on colloidal TiO_2 films deposited on PES.

2. Results and discussion

2.1. Effect of sunlight compared with visible light on the bacterial inactivation kinetics on polyester–TiO_2: monitoring the high-oxidized radicals

Figure 1 shows the *E. coli* inactivation kinetics as a result of bacterial degradation of diverse RF-pretreated PES samples under Osram Lumilux lamp irradiation emitting at 4.1 mW cm^{-2}. Trace 1 presents the almost negligible disinfection action of the PES sample by itself. Trace 2 shows a PES–TiO_2 sample without pretreatment inactivating bacteria within 5 h. Traces 3, 4 and 5 present a faster *E. coli* inactivation as the pretreatment time increases from 10 up to 30 min. The faster bacterial reduction kinetics within 1.5 h for PES–TiO_2 samples pretreated for 30 min involves an increased amount of oxidative radicals (mainly OH radicals) developed on the PES–TiO_2 [17]. Trace 6 shows that the 120 min RF-pretreatment period does not shorten the bacterial reduction kinetics beyond that shown by a 30 min RF pretreatment. Therefore, the capacity to produce highly oxidative radicals (OH radicals) seems to reach a maximum after 30 min of RF-plasma.

Figure 2*a* presents the fluorescence intensity of PES samples pretreated with RF-plasma for different times after 30 min of illumination. These results show the favourable effect of an increase in RF-plasma pretreatment time up to 30 min for PES–TiO_2 samples, enhancing OH radical generation upon illumination. The OH radicals produced on the PES–TiO_2 have been quantified by measuring the fluorescence of the terephthalic acid [18,19]. Upon illumination of the PES–TiO_2, the terephthalic acid in NaOH solution converts to a highly fluorescent hydroxy-substituted product. Monitoring the increase of the

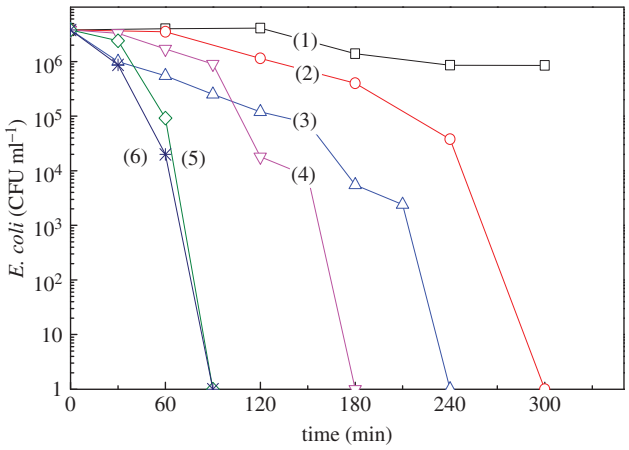

Figure 1. *Escherichia coli* inactivation kinetics of RF-plasma PES-pretreated samples irradiated by actinic light for different times: (1) PES alone, (2) PES–TiO_2 not RF-plasma treated sputtered for 8 min, (3) samples sputtered for 8 min and RF-plasma pretreated for 10 min, (4) RF-plasma pretreated for 20 min, (5) RF-plasma pretreated for 30 min and (6) RF-plasma pretreated for 120 min. (Online version in colour.)

hydroxy product allows the TiO_2 surface-generated oxidative species (OH radicals) to be estimated. We can only suggest that the active sites on the RF-pretreated PES–TiO_2 are introduced from two sources: (i) by the RF pretreatment of the PES generating polar binding sites due to the residual O_2 in the RF treatment cavity and (ii) by the impurities, defects and dangling bonds of the interfacial PES–TiO_2 (anatase).

The actinic Osram Lumilux 18 W/827 lamp acts as a simulated sunlight source to activate the PES–TiO_2 sample fluorescence. Figure 2*b* presents the lamp emission spectrum between 320 and 730 nm with an integral output of 4.1 mW cm^{-2}.

The diffuse reflectance spectroscopy (DRS) spectra for the PES–TiO_2 RF-pretreated samples for 10, 20 and 30 min are shown in figure 3. The light absorption of the PES alone is due to the TiO_2 content added as whitener during the fabrication of PES as described in the Material and methods section.

The spectra in figure 3 show the direct relationship between the light absorption in Kubelka–Munk units as a function of the RF-plasma pretreatment time. The approximate UV-Vis reflectance data cannot be used directly to assess the absorption coefficient of the RF-pretreated samples because of the large scattering contribution to the reflectance spectra. Normally, a weak dependence is assumed for the scattering coefficient S on the wavelength. In figure 3, the scattering coefficient S is a function of the spectral wavelength in the DRS spectra. The KM/S values for the samples in figure 3 follow the same trend observed for the bacterial reduction kinetics reported previously in figure 1.

The wt% Ti/wt PES in table 1 shows the increases in TiO_2 content with a longer RF-plasma pretreatment time.

Figure 4*a* presents the fluorescence of the PES–TiO_2 samples irradiated for up to 30 min by an Osram Lumilux 18 W/827 lamp using a 400 nm cut-off filter as shown in the inset in figure 4*a*. Figure 4*a* shows a drastic fluorescence reduction with respect to the same data presented in figure 2*a*. The residual fluorescence induced by the filtered light of the Osram Lumilux 18 W/827 lamp comes from the tail optical absorption of the PES–TiO_2 between 400 and 500 nm (figure 3). The tail optical absorption involves C–TiO_2 bands with a yellow colour introduced on the PES surface during the RF pretreatment. The C–TiO_2 species have been reported as being responsible for optical absorption above 400 nm [19,20]. The

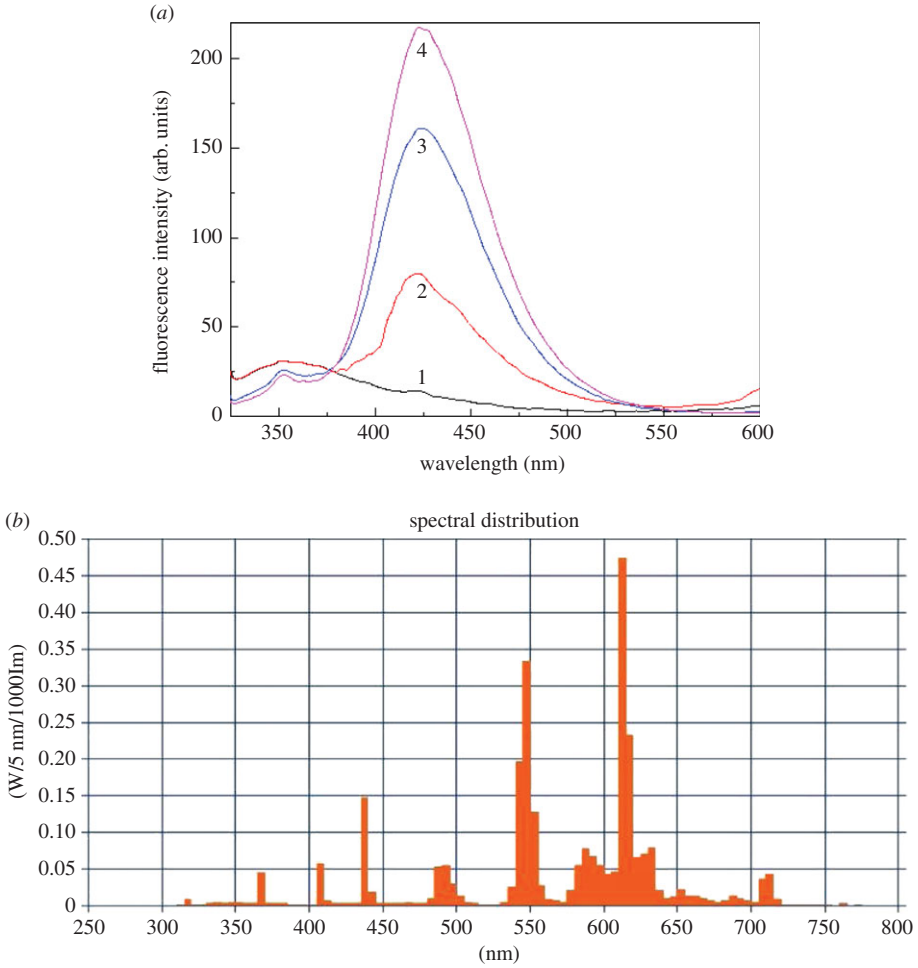

Figure 2. (*a*) Fluorescence intensity versus wavelength for PES–TiO_2 samples sputtered for 8 min and pretreated for: (1) zero, (2) 10 min, (3) 20 min and (4) 30 min. Samples were irradiated for 30 min by an actinic Osram Lumilux 18 W/827 lamp. For more details see text. (*b*) Spectral distribution of the actinic lamp Osram Lumilux 827/18 W (Winterthur, Switzerland). (Online version in colour.)

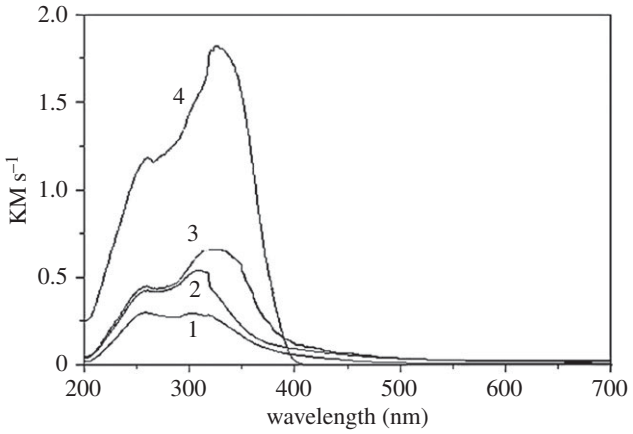

Figure 3. Diffuse reflectance spectroscopy (DRS) of PES–TiO_2 samples sputtered for 8 min. The PES was RF-plasma pretreated for: (1) zero, (2) 10 min, (3) 20 min and (4) 30 min.

Table 1. X-ray fluorescence determination of PE–TiO_2 sputtered for different times with and without PE pretreatment for the times indicated.

sample	surface TiO_2 wt %/wt PE
PE–TiO_2 (1 min), no pretreatment	0.009
PE–TiO_2 (3 min), no pretreatment	0.019
PE–TiO_2 (5 min), no pretreatment	0.031
PE–TiO_2 (8 min), no pretreatment	0.051
PE–TiO_2 (8 min), RF plasma pretreated under vacuum 15 min (1 torr)	0.081
PE–TiO_2 (8 min), RF air plasma pretreated for 15 min	0.096

RF pretreatment introduces C-oxidative functionalities on the PES and the local heat effects break the PES intermolecular H-bonds [21]. The evaporation of water from the PES leaves spaces for the diffusion of TiO_2 into the PES matrix, which increases with the RF-plasma pretreatment time [22]. Figure 4*b* shows the bacterial I reduction kinetics in the presence of the cut-off filter 400 nm. The inactivation kinetics is slowed to 3.5 h, providing further evidence for the generation of a small amount of highly oxidative radicals when a 400 nm cut-off filter is used to inactivate bacteria only using visible light irradiation (filtered light conditions).

2.2. Surface characterization of polyester–TiO_2 surfaces

Figure 5*a* presents the transmission electron microscopy (TEM) of: (i) the PES surface sample and (ii) the PES–TiO_2 where a

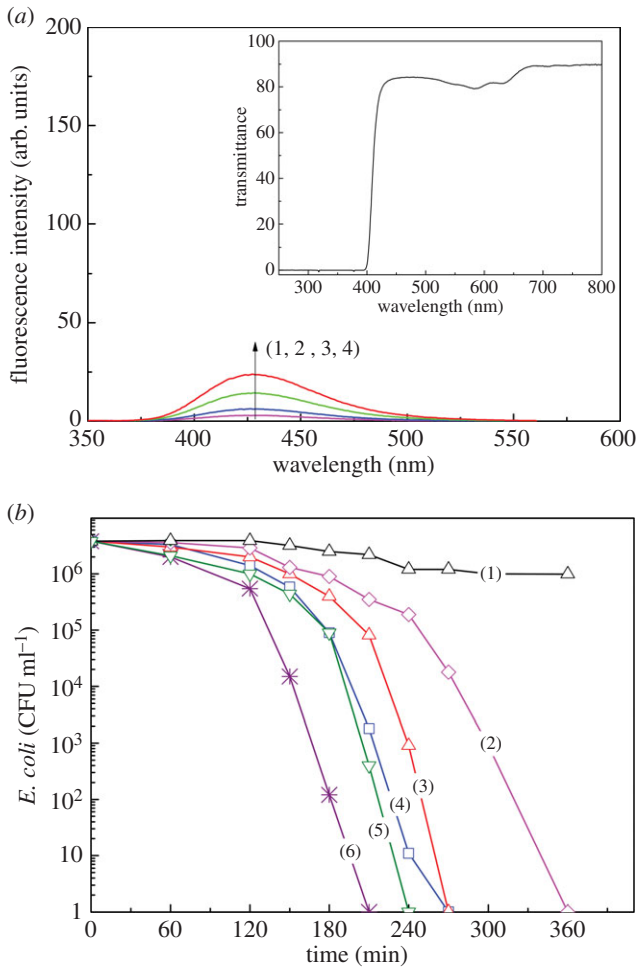

Figure 4. (*a*) Fluorescence intensity versus wavelength for PES–TiO_2 sputtered for 8 min on RF-pretreated samples for: (1) zero, (2) 10 min, (3) 20 min and (4) 30 min. Samples were irradiated for 30 min by an actinic Osram Lumilux 18 W/827 lamp using a 400 nm filter as shown in the insert. (*b*) *E. coli* inactivation PES–TiO_2 samples sputtered for 8 min and irradiated by an actinic Osram Lumilux 827/18 W lamp in the presence of the 400 nm filter shown in figure 4*a*: (1) PES alone, (2) PES–TiO_2 non-pretreated (3) RF-plasma PES–TiO_2 samples pretreated for 10 min, (4) 20 min, (5) 30 min and (6) 120 min. (Online version in colour.)

continuous coating between 25 and 80 nm thick of TiO_2 is observed for the RF-plasma-pretreated sample. Un-aggregated particles show sizes between 20 and 30 nm. This means that the coating in figure 5*a* comprises between one and four TiO_2 layers.

Figure 5*b* shows the X-ray diffraction for PES and for PES–TiO_2 RF-plasma-pretreated samples for 30 min. A strong signal for anatase is readily seen at 25.2° along with smaller anatase satellite peaks.

Figure 5*c* shows the X-ray electron spectroscopy (XPS) deconvoluted spectrum of an RF-plasma-pretreated PES–TiO_2. The peaks for the OH group at 531.0 eV [23], Ti–O at 529.8 eV [24] and the Ti–O–C peak at 532.8 eV [25] are shown in figure 5*c*. A large amount of adsorbed/chemisorbed water was introduced in the sample during the sol–gel coating at temperatures less than or equal to 100°C. The amount of surface OH_{surf} radical adsorbed on the sample is higher after the RF-plasma pretreatment due to the increased hydrophilicity introduced by the O-containing polar groups by the RF-plasma pretreatment.

2.3. Transparent, non-scattering polyethylene–TiO_2 sputtered films inactivating *Escherichia coli*: reversible photo-switching required for repetitive disinfection processes

Recently, a report addressed the synthesis, kinetics and characterization of TiO_2 transparent non-scattering films able to inactivate *E. coli* within the minute range [26]. Figure 6 shows *E. coli* inactivation on PE–TiO_2 films under simulated solar light with a dose of 52 mW cm^{-2}. The fastest bacterial inactivation was found for pretreated PE–TiO_2 samples sputtered for 8 min and RF-plasma PE pretreated for 15 min. No significant bacterial inactivation was observed for bacteria on uncoated PE. These sputtering and pretreatment times lead to the most favourable bacterial inactivation kinetics by PE–TiO_2 films. The bacterial evaluation procedure used was carried out according to [27]. The RF-plasma allowed the sputtering of additional uniform TiO_2 layers compared with non-pretreated PE. The PE–TiO_2 samples pretreated for 15 min and sputtered for 8 min presented the highest amount of TiO_2 sites in exposed positions leading to the favourable bacterial inactivation kinetics shown in figure 6, trace 1 [25]. PE–TiO_2 sputtered samples for times between 1 and 5 min were not loaded with sufficient TiO_2 to result in rapid bacterial inactivation. The loading weights of TiO_2 on PES on transparent TiO_2–PE films are shown in table 1.

Samples sputtered for times longer than 8 min led to a thicker coating inducing charge bulk inward diffusion decreasing the charge transfer between the PE–TiO_2 and bacteria [28]. It seems that the TiO_2 sputtering for 8 min leads to a TiO_2 loading with the most suitable thickness for the charge diffusion generated in the TiO_2 reaching the bacteria. To verify that no re-growth of *E. coli* occurs after the first bacterial inactivation cycle, the PE–TiO_2 film was incubated on an agar Petri dish for 24 h at 37°C. No bacterial re-growth was observed, meaning that no bacteria adhered to the surface after the inactivation cycle.

The bacterial inactivation for the most suitable PE–TiO_2 samples (PE pretreated with RF-plasma in air for 15 min then TiO_2 sputtered for 8 min) was investigated up to the sixth cycle. The recycling of the sample showed a stable inactivation kinetics up to the fifth cycle, afterwards slowing down by approximately 20%. After each cycle, the samples were washed with distilled water and dried. Then, samples were kept in an oven at 60°C to avoid bacterial contamination. After washing, the PE–TiO_2 samples were left standing for 24 h before regaining the initial sample hydrophobicity. This will be discussed below since it relates to PE–TiO_2 film hydrophobic–hydrophilic transformation under sunlight irradiation and the reverse dark reaction. This is shown below by the hydrophobic–hydrophilic transformation under light shown in figures 7*a*,*b* and 8.

Figure 7*a* illustrates the rate at which the hydrophilicity is photo-induced up to 60 min on PE–TiO_2. Figure 7*b* shows the restoration rate of the initial hydrophobicity found on the PE–TiO_2 surfaces in the dark as a function of cos θ. The rate of change of hydrophobic to hydrophilic was found to be 0.277 min^{-1} and the reverse reaction rate was 8.71×10^{-3} min^{-1}. The reverse reaction was complete within 24 h. These rates were calculated by integrating cos θ in Young's equation [7,8,16,28,29].

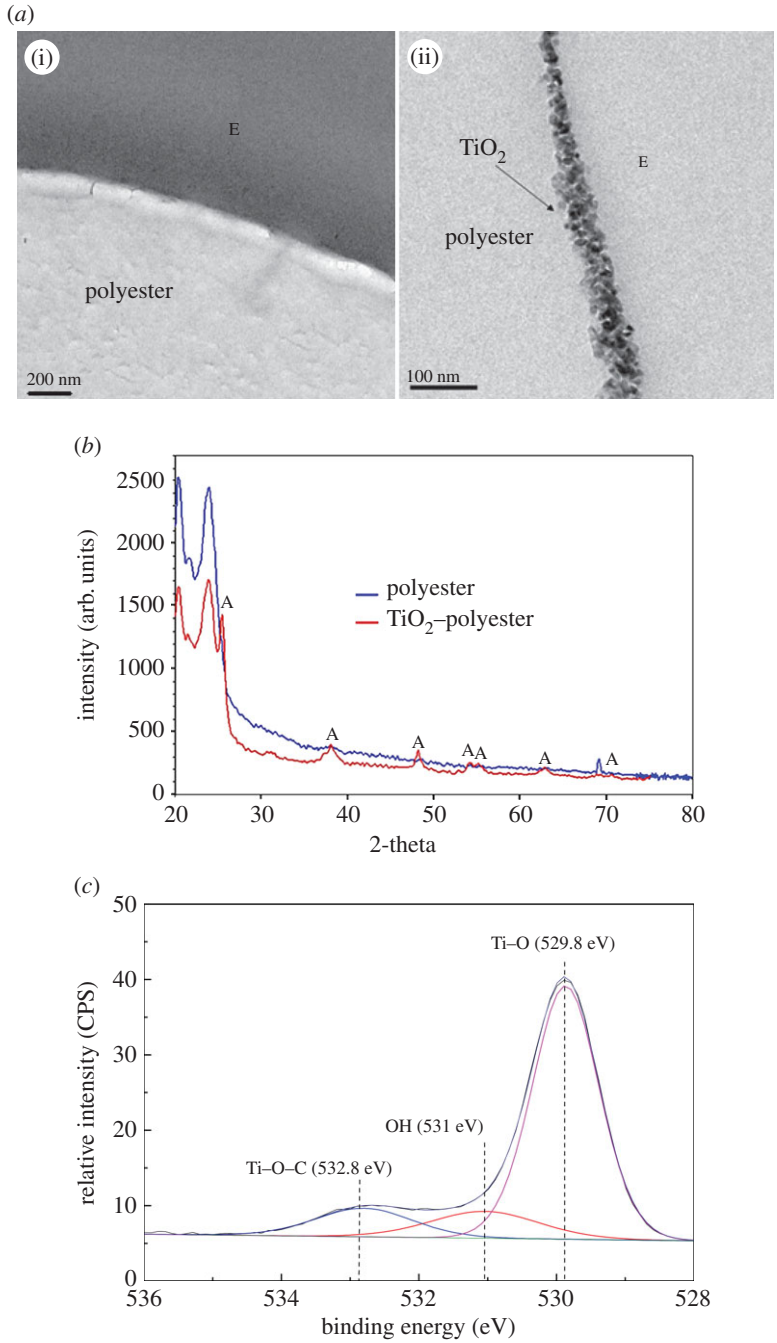

Figure 5. (*a*) TEM of (i) PES and (ii) PES–TiO_2 sputtered for 8 min after RF-plasma pretreatment for 30 min (E indicates the epoxide used in the preparation and cutting of the sample). (*b*) X-ray diffraction of PES (lower trace) and an RF-plasma pretreated PES–TiO_2 sample pretreated for 30 min and sputtered for 8 min with TiO_2. For more details see text. (*c*) XPS O1s spectra of PES–TiO_2 sputtered for 8 min and RF-pretreated showing the bands assigned to Ti–O, Ti–O–C and the OH_{surf} functionalities.

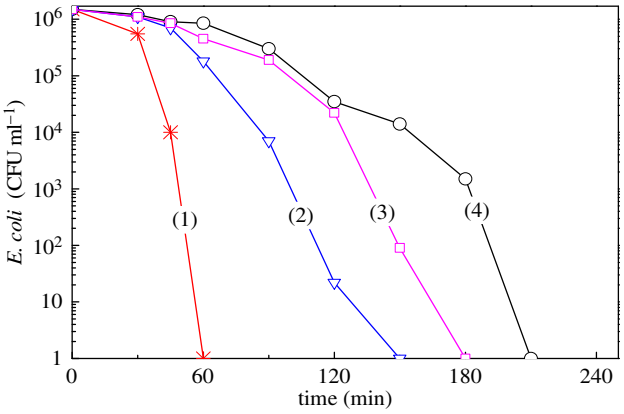

Figure 6. PE–TiO_2 samples sputtered for 8 min after RF air plasma pretreatment for: (1) 15 min, (2) 20 min, (3) 30 min and (4) 5 min.

According to Young's theory the cos θ of a liquid droplet on a solid is a function of the interfacial energy between the solid and the liquid. The wettability is commonly evaluated in terms of the contact angle (CA), which is given by Young's equation [29] as

$$\gamma_S = \gamma_{SL} + \gamma_L \cdot \cos\theta, \tag{2.1}$$

where γ_S and γ_L are the surface free energies per unit area of the solid and liquid, respectively, and γ_{SL} is the interfacial free energy per unit area. In addition, γ_{SL} can be approximated using the Girifalco–Good equation (2.2), with γ_S and γ_L, as

$$\gamma_{SL} = \gamma_S + \gamma_L - \Phi\left(\frac{\gamma_S}{\gamma_L}\right)^{1/2}. \tag{2.2}$$

Here, Φ is a constant parameter ranging from 0.6 to 1.1, depending on the solid. In addition, γ_L is the water surface

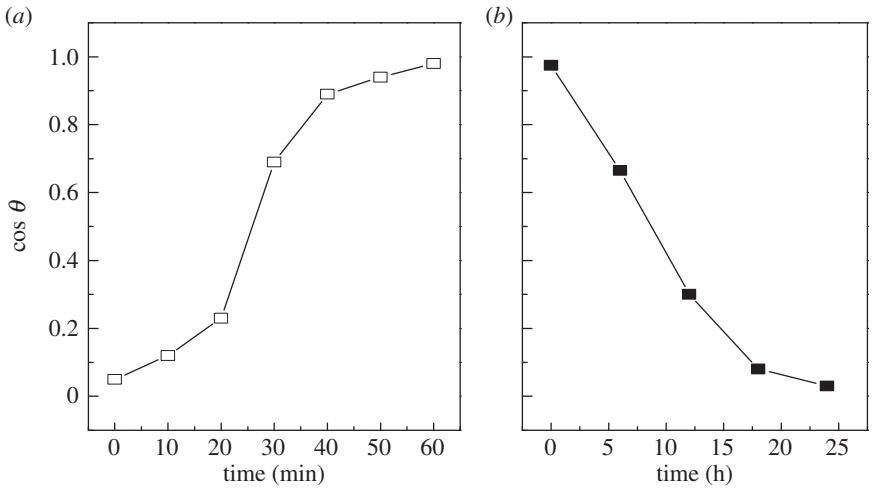

Figure 7. (*a*) The hydrophobic–hydrophilic kinetics for a PE–TiO_2 sample sputtered for 8 min after being RF air plasma pretreated for 15 min under solar simulated light and (*b*) kinetics of the dark reverse reaction for the same sample.

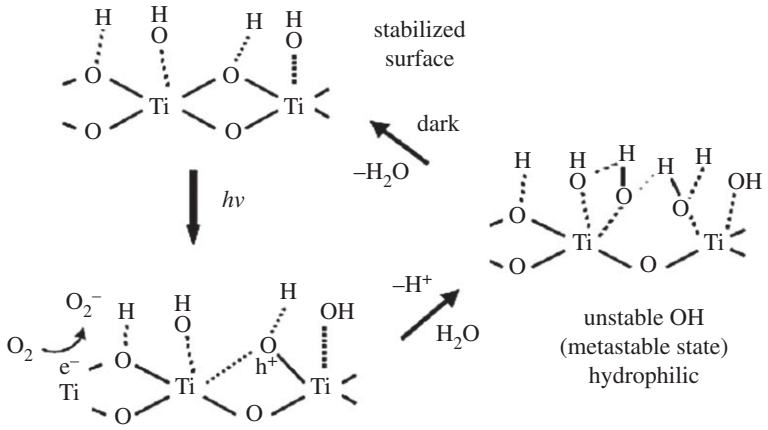

Figure 8. TiO_2 hydrophobic to hydrophilic conversion under solar simulated light showing the TiOH metastable state on the TiO_2 surface (for details see [29,30]).

free energy, which has a constant value of 74 mJ m^{-2}. Therefore, by combining (2.1) and (2.2), the CA can be simply expressed as

$$\cos\theta = c\gamma S^{1/2} - 1(\mathbf{c}\text{:const.}). \tag{2.3}$$

The highly hydrophilic state generated by UV light gradually returns to the initial hydrophobic state in the dark, as shown in figure 7*b*. The hydrophobic nature of the PE–TiO_2 surface before the photo-switching is important for the performance of the antibacterial films. Under light the mechanism of the hydrophilic conversion can be explained on the basis of the evidence found by electrochemical experiments [30]. These experiments show that the photo-generated holes, not the electrons under light irradiation, led to the hydrophilic conversion shown in figure 8. The photo-generated holes in the bulk diffuse to the TiO_2 surface and are trapped at the lattice oxygen sites. The trapped holes react with the adsorbed organics directly, or are adsorbed in water producing OH radicals. However, a small portion of the trapped holes reacts with TiO_2, breaking the bond between the lattice Ti and oxygen ions and coordinating with water molecules at the Ti site [29]. The coordinated water molecules release a proton for charge compensation and then a new OH group forms, leading to the increase in the number of OH groups at the TiO_2 surface. The TiO_2 surface is gradually covered with the thermodynamically less stable OH groups, which have a higher energy than that of the TiO_2 surface covered with the initial OH groups.

The initial CA in figure 7*a* decreased to a CA less than 5° within 60 min of irradiation. The hydrophobic or hydrophilic nature of a surface is important in the adhesion of the bacteria to a surface and the subsequent light- or dark-induced inactivation. *Escherichia coli* and *Staphylococcus aureus* present a preferential adhesion to hydrophilic surfaces [16,31,32]. Bacteria with hydrophobic surface properties such as *Staphylococcus epidermidis* adhere preferentially to hydrophobic surfaces [33]. Hydrophobic bacteria have been reported to adhere to a variety of surfaces forming biofilms to a greater extent than hydrophilic bacteria [34]. Recently, Amal and co-workers have reported reversible photo-switching behaviour under light by Ag nanoparticles [35,36].

2.4. Surface characterization of polyethylene–TiO_2 films

2.4.1. Atomic force microscopy topography of polyethylene–TiO_2 sputtered films

Figure 9 presents PE–TiO_2 RF air plasma-pretreated samples: rugosity = roughness = R_g = 7 nm was observed for PE–TiO_2 sputtered for 8 min, without PE pretreatment. A larger R_g value of 16 nm was observed for PE–TiO_2 sputtered for 8 min and pretreated for 15 min at 1 torr. The value for PE–TiO_2 pretreated by RF air plasma for 15 min and sputtered for 8 min was R_g = 11 nm. The roughness values for different PE samples were observed to be higher for pretreated samples than for non-pretreated samples. The general trend observed was that higher roughness leads to

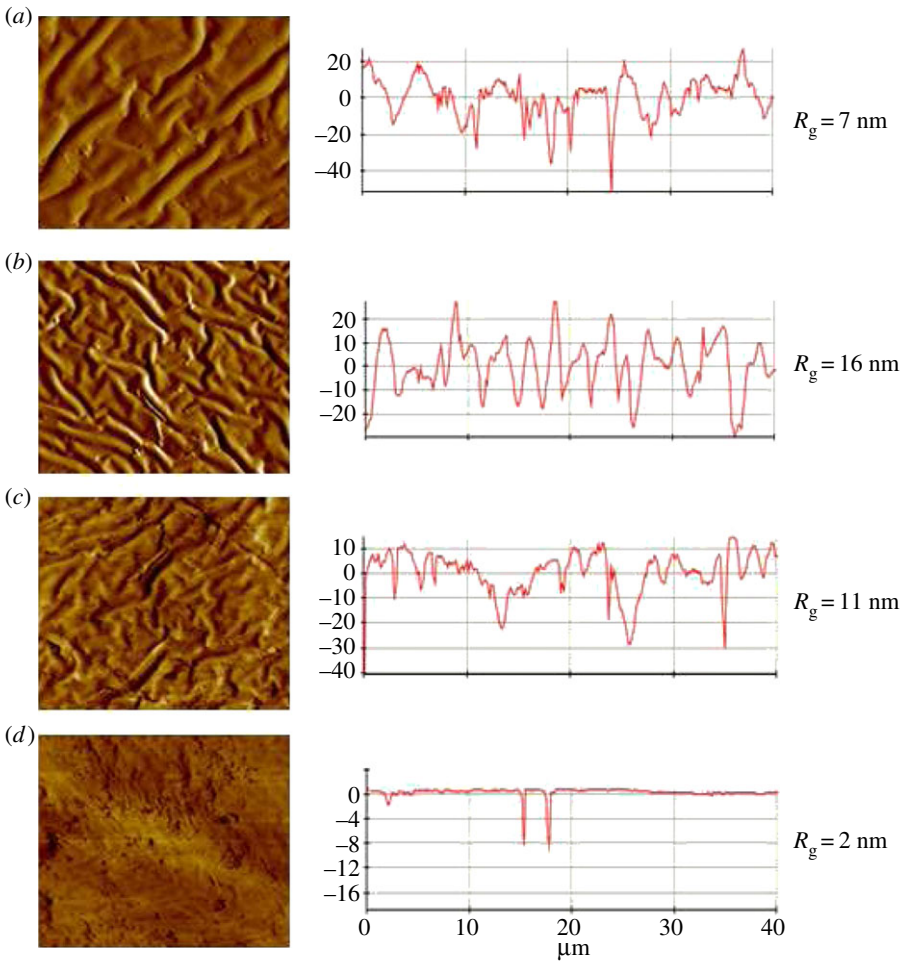

Figure 9. Atomic force microscopy topography of PE–TiO_2 samples: (*a*) PE–TiO_2 sputtered for 8 min no pretreatment, (*b*) PE–TiO_2 sputtered for 8 min and RF-plasma pretreated at 1 torr for 15 min, (*c*) PE–TiO_2 sputtered for 8 min and RF air plasma pretreated for 15 min, (*d*) PE–TiO_2 sputtered for 1 min and RF air plasma pretreated for 15 min. (Online version in colour.)

a faster bacterial inactivation and also involved thicker TiO_2 layers.

2.4.2. Transmission electron microscopy and energy dispersive X-ray spectroscopy of polyethylene–TiO_2 surfaces

Figure 10*a–d* shows the scanning electron microscopy (SEM) images for PE–TiO_2 RF air plasma pretreated for 15 min and sputtered for 8 min, inducing faster bacterial inactivation (figure 6). Figure 10*a* show a continuous coating of TiO_2 on PE. A TiO_2 thickness of approximately 60 nm is equivalent to 300 layers, taking an atomic layer thickness of 0.2 nm. Figure 10*b* shows high-angle annular dark-field (HAADF) scanning electron microscopy. The uniform distribution obtained by energy dispersive X-ray spectroscopy (EDX) of O and Ti on the coating is shown in figure 10*c* and *d*.

2.4.3. Redox processes at the polyethylene–TiO_2 surface detected by X-ray photoelectron spectroscopy

Figure 11*a*,*b* shows the deconvoluted O1 s peaks of PE–TiO_2 films with no pretreatment and after pretreatment. The peaks of the Ti–O, Ti–OH and O–C bands for non-pretreated PE–TiO_2 are shown in figure 11*a*. Figure 11*b* presents the deconvoluted O1 s bands of PE–TiO_2 pretreated in air plasma for 15 min showing a shift greater than 0.2 eV for the Ti–O, Ti–OH and O–C bands due to redox processes occurring during the RF-plasma air sample pretreatment. The Ti–O and Ti–OH species in the XPS spectrogram were deconvoluted by introducing the sensitivity factors for oxygen [23,37,38]. The Ti–OH on PE–TiO_2 samples show peaks at 532.4 and 532.7 eV. The PE pretreatment gives rise to a different O–C boundary layer between PE and TiO_2, introducing a different accessibility for the attachment of TiO_2 to PE [39,40].

The different pretreatments of PE give rise to boundary O–C layers allowing the PE–TiO_2 films to react in a specific way during bacterial inactivation. The different bacterial kinetics observed for the PE–TiO_2 samples during the bacterial inactivation kinetics is possibly due to: (i) different accessibility of the bacteria to the O–C catalytic sites on the PE–TiO_2 and (ii) different distances between the interfacial layers and bacteria [25].

Redox processes involve Ti^{4+}/Ti^{3+} species on PE–TiO_2 during the photocatalytic bacterial inactivation. This is shown next in figure 11*c*,*d*. At time zero, figure 11*c* shows the Ti^{4+} peak at 458.6 eV. This binding energy value is slightly higher than the Ti^{3+} peak at 457.8 eV, with both oxidation states coexisting on the PE–TiO_2 sample. But after bacterial inactivation, the Ti^{3+} peak in figure 11*d* amounts to more than 90% of the XPS signal and the Ti^{4+} to less than 10%. This redox reaction on the TiO_2 occurs concomitantly to the increase in hydrophilicity within 60 min required for bacterial inactivation on PE–TiO_2 samples (figure 7).

2.5. On the kinetics and mechanism of the bacterial inactivation in the dark with TiO_2 surfaces

The TEM of the PES–TiO_2 interaction with *E. coli* is shown in figure 12. The TEM in figure 12*a* shows the interaction of the

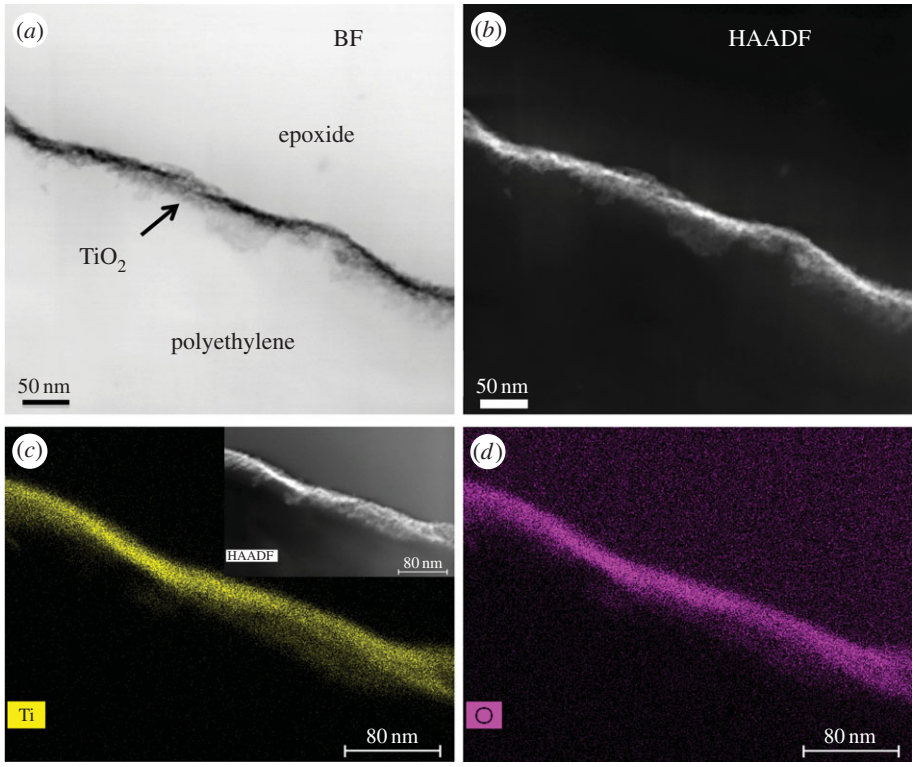

Figure 10. (*a*) SEM of an PE–TiO_2 sample RF air plasma pretreated for 15 min and sputtered for 8 min (BF, bright field), (*b*) HAADF image taken on the same sample, (*c*) EDX mapping of Ti of this sample and (*d*) EDX mapping of O. For more details see text.

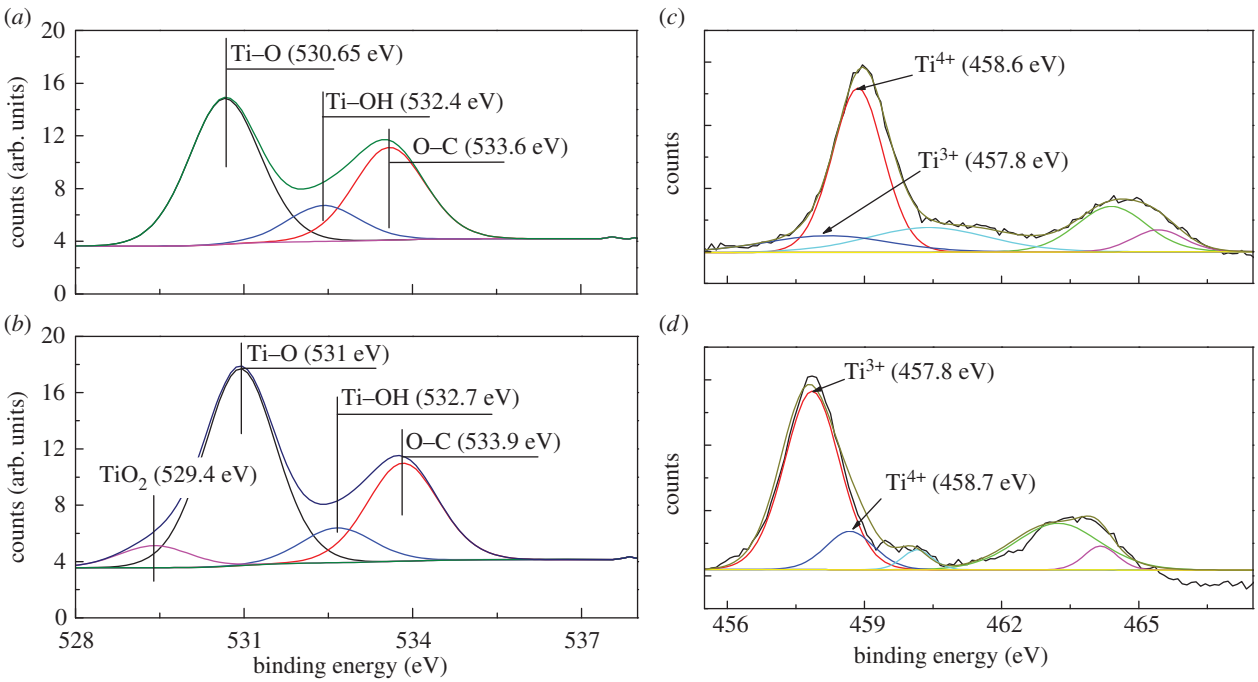

Figure 11. (*a*,*b*) O1 s deconvolution of PE–TiO_2 XPS spectral peaks for samples sputtered for 8 min and: (*a*) no pretreatment, (*b*) after RF air plasma pretreatment for 15 min. (*c*,*d*) Ti2p peak deconvolution of a PE–TiO_2 sample sputtered for 8 min and pretreated with RF air plasma for 15 min (*a*) before and (*b*) after bacterial inactivation under solar simulated light involving Ti^{3+}/Ti^{4+} oxidation states within 60 min, the bacterial inactivation period.

TiO_2–PET sample with *E. coli* K12 at time zero. The *E. coli* intact cell wall is seen as well as the aggregates and co-aggregates of TiO_2 positioned at a distance from the cell wall in agreement with the Derjaguin–Landau–Verwey–Overbeek theory of colloidal stability. TiO_2 nanoparticle aggregation commences at a pH close to the isoelectric point (IEP) of 6.8 due to the attractive van der Waals forces leading to TiO_2 aggregation within 30 min as shown in figure 12*b* [41]. The TiO_2 single particles present sizes between 40 and 60 nm and the hydrodynamic diameters of the aggregates were found to be 170–240 nm, i.e. equivalent to three or four primary TiO_2 particles. After 30 min, the TiO_2 aggregates accumulate on the cell wall surface due to their almost neutral charge at physiological pH as shown in

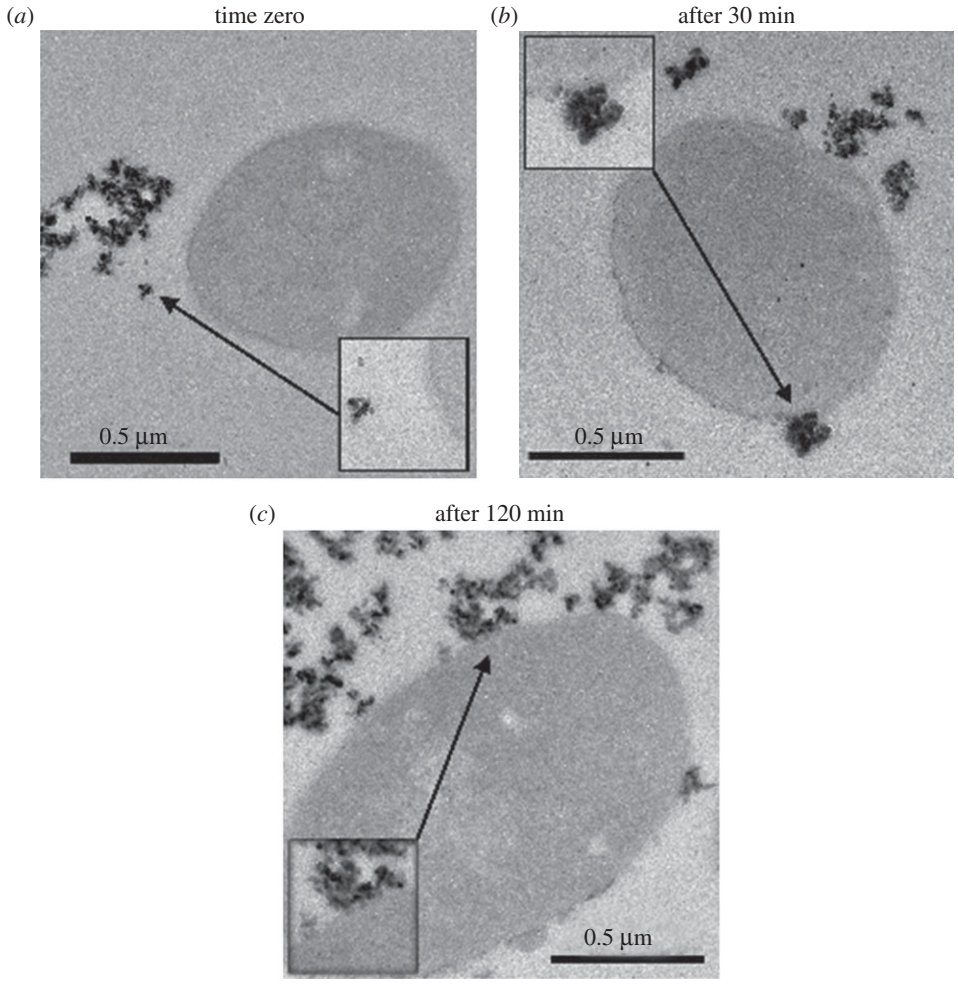

Figure 12. TEM of TiO_2–PES 5% (hydrothermal) interacting with the *E. coli* cell wall in the dark at (*a*) time zero (*b*) time 30 min (*c*) time 120 min. For more details, see text.

figure 12*b*. A weak attraction between the TiO_2 (IEP approx. 6.8) and the negatively charged cell wall commences at a pH close to the TiO_2 IEP of 6.8. The weak electrostatic interaction between the co-aggregates of TiO_2 and the negative bacterial cell wall in the dark within 30 min seems to attach the TiO_2 NP's to the cell wall.

Figure 12*c* shows the damage to the *E. coli* outer wall cell within 120 min. After 120 min, the wall outer layers show discontinuities and have vanished in some regions. The observed damage to the cell wall leading to cell inactivation involves changes to the cell morphology, cell microstructure and local pH that have been reported previously (P. Vadgama 2014, personal communication). Damage to the cell wall due to abrasion by the TiO_2 rutile component on the *E. coli* envelope has also been reported [42]. The extensive damage in the outer cell layers after 120 min in the dark coincides with the time required for the total loss of cell viability shown in figure 12*c*. The bacterial cell cannot function anymore as a membrane regulating the equilibrium osmotic pressure and material flow. Sunada *et al*. [43] reported *E. coli* inactivation by TiO_2 films due to damage to the cell wall membrane leading to the leakage of internal cell components.

2.6. Summary

This study describes the preparation of PES–TiO_2 and PE–TiO_2 films and the evaluation and characterization of bacterial reduction under light and in the dark. The films were sputtered at temperatures compatible with non-heat-resistant textiles (PES) and polymer films (PE). The TiO_2 films were observed to be uniform and adhesive. The microstructure of the TiO_2 surfaces was characterized by common surface techniques. The interaction of TiO_2 films in the dark with bacteria was followed in the time scale by way of TEM. This is important since almost all studies address exclusively bacterial inactivation by TiO_2 photocatalysis. RF-plasma was shown to be necessary to increase the number of surface active sites able to bond TiO_2. TEM of the TiO_2 sputtered films shows a continuous coating of TiO_2. By XPS, evidence was found for the destruction of bacterial residues and redox catalysis occurring during bacterial inactivation enabling the sample to inactivate a new bacterial charge at the end of the disinfection process. The damage to the *E. coli* outer layers by PES–TiO_2 in the dark is shown to proceed stepwise leading to complete bacterial inactivation within 120 min. Inactivation proceeds within 60 min under solar simulated light.

The nanoparticle films described in this study are a topic of increasing attention since they can reduce/eliminate the formation of infectious bacteria biofilms leading to HAIs. These nosocomial infections due to antibiotic-resistant bacteria have become more frequent during the last decade and contribute to the increasing cost of hospital care. The disinfecting surfaces as prepared in this study should decrease the microbial density in hospital facilities since there was no re-growth of bacteria on the PE–TiO_2 films prepared during the course of this study. This observation warrants further work on antibacterial surfaces since they seem to present a practical potential to

preclude pathogenic biofilm formation in the dark and at a faster rate under band-gap light irradiation.

3. Material and methods

3.1. Radio-frequency plasma samples pretreatment, DC-sputtering, X-ray fluorescence, diffuse reflectance spectroscopy and contact angle

RF-plasma samples pretreatment. The procedure has been describe recently [17,22,25]. The PET polyester Dacron EMPA test cloth no. 407 fabric was pretreated in the vacuum cavity of the RF-plasma unit at approximately 1 torr and also at atmospheric pressure in the cavity of an RF-plasma unit (Harrick Corp., 13.56 MHz, 100 W).

Sputtering procedures. The TiO_2 was sputtered by direct current magnetron sputtering (DC) as reported previously [17,44]. The reactive DC-magnetron sputtering used a 5 cm diameter Ti target that was 99.99% pure (Kurt J. Lesker, Hastings, UK) in an O_2 gas flow. The current on the Ti target was set at 280 mA (power of 128 W). Before sputtering the films, the pressure P_r in the sputtering chamber was set to $P_r = 10^{-4}$ Pa. The substrate to target distance was set at 10 cm. The thickness of the sputtered layers was determined by means of a profilometer (Alphastep500, Tencor) for films onto silica wafers in the magnetron chamber.

X-ray fluorescence (*XRF*). The Ti content on the PES was evaluated by XRF since it emits an X-ray of a certain wavelength associated with the particular atomic number in the PANalytical PW2400 spectrometer.

DRS was carried out using a Perkin Elmer Lambda 900 UV-VIS-NIR spectrometer with a PELA-1000 accessory within the wavelength range of 200–800 nm and a resolution of 1 nm. The absorption of the samples was plotted in Kubelka–Munk (KM/S units) versus wavelength.

Contact angle. The CA of TiO_2 films was determined by the sessile drop method on a DataPhysics OCA 35 unit. FTIR spectra were measured in a Portmann Instruments AG spectrophotometer equipped with a Specac attachment.

3.2. Bacterial inactivation evaluation, irradiation procedures and determination of the OH radical by fluorescence spectroscopy

Bacterial inactivation evaluation. The samples of *Escherichia coli* (*E. coli* K12) were obtained from Deutsche Sammlung von Mikroorganismen und Zellkulturen GmbH (DSMZ) ATCC23716, Braunschweig, Germany. A total of 100 µl culture aliquots with an initial concentration of approximately 106 CFU ml^{-1} in NaCl/KCl (pH 7) were placed on coated and uncoated (control) PE fabric. The 100 µl of the *E. coli* solution was placed in contact with the TiO_2 uniform films. The distribution of bacteria on the substrate turned out to be homogeneous and was in contact with the inoculated cells. The procedure was carried out at ambient temperature. The samples were then placed on Petri dishes with a lid to prevent evaporation. After each determination, the fabric was transferred into a sterile 2 ml Eppendorf tube (900 µl) containing autoclaved NaCl/KCl saline solution. This solution was subsequently mixed thoroughly using a vortex for 3 min. Serial dilutions were made in NaCl/KCl solution. A sample of 100 µl of each CFU run was pipetted onto a nutrient agar plate and then spread over the surface of the plate using standard plate method. Agar plates were incubated lid down, at 37 °C for 24 h before colonies were counted. Three independent assays were done for each sputtered sample. The CFU statistical analysis was performed by calculating the standard deviation values. The average values were compared by one-way analysis of variance and with the value of statistical significance. The one-way analysis of variance (one-way ANOVA) was used to compare the mean of the samples using the Fisher distribution. The response variable was approximated for the sample data obtained from the photocatalytic inactivation of test samples presenting the same distribution within the same sputtering time. The bacterial evaluation method used has been reported previously to test the antibacterial activity of the PES–TiO_2 fabrics [17,44]. The bacterial data reported were replicated three times. To verify that no re-growth of *E. coli* occurred after the total inactivation observed in the first disinfection cycle, the samples were incubated for 24 h at 37°C, and replica samples were incubated at 37°C for 24 h at the end of each bacterial inactivation cycle. No bacterial re-growth was observed.

Irradiation procedures. The irradiation of the samples was carried out in the cavity of a reactor provided with reflecting Al walls irradiating by way of a Osram Lumilux 18 W/827 lamp with light emission resembling the solar spectrum (figure 3). A filter at 400 nm was introduced to filter the light that was not in the visible range of more than 400 nm.

Detection of the OH radicals was carried out according to recent work reported by Hashimoto and colleagues [18] and Girault and colleagues [19]. A sample of 4 cm^2 of TiO_2-coated fabric was immersed in a solution of terephthalic acid at 0.4 mM dissolved in a 4 mM NaOH solution. After each irradiation, the solution was transferred into a quartz cell and the fluorescence spectra of 2-hydroxyterephthalic were measured on a Perkin Elmer spectrometer at 450 nm under an excitation wavelength of 315 nm.

3.3. Atomic force microscopy, transmission electron microscopy, X-ray diffraction and X-ray photoelectron spectroscopy

Atomic force microscopy (*AFM*). The AFM images were acquired in contact mode using a PSIA Xe-100 atomic force microscope. Silicon nitride cantilevers were used with feedback set points around 1.0 nN. The images originate from the Z-scanner (12 µm) and are not influenced by the nonlinearity and the hysteresis of the Z-scanner. The roughness values involve an experimental error below 10%. The mean surface roughness (Ra) was calculated for the scanned area by applying the equation:

$$\mathrm{Ra} = \sqrt{\sum_{x,y}^{N} \frac{(Z_{x,y} - Z_{\mathrm{average}})^2}{N^2}},$$

where Ra is the normalized standard deviation calculated from the local heights ($Z_{x,y}$) and the average height (Z-average) determined over the x,y coordinates (N) measured in the AFM image.

TEM. A CM12 microscope at 120 kV was used to follow the PES–TiO_2 coating interaction with bacteria as a function of time. The samples were embedded in epoxy resin 45 359 Fluka and the fabrics were cross-sectioned with an ultramicrotome (Ultracut E) at an angle of 35°. HAADF imaging was used to map the scanning transmission electron microscopy (STEM) using a FEI Tecnai TEM-STEM OSIRIS, 200 kV. The Z-contrast images were obtained by collecting the scattered electrons passing through the objective provided with an annular dark field.

To take the TEM images showing the interaction of bacteria with PES–TiO_2, the *E. coli* were fixed in paraformaldehyde 2% + glut 0.2% in phosphate buffer for 30 min, centrifuged and the pellet was re-suspended in low melting point agarose. The sample was then cut into small cubes, dehydrated and stained for 20 min in 2% uranyl-acetate, then dehydrated in graded

alcohol. The samples were then embedded in the LR white resin in beam capsules and polymerized overnight at 55°C. The resin blocks containing the *E. coli* on the PES–TiO_2 were sectioned with an ultramicrotome (Leica UC7). The PES–TiO_2 fibres were embedded in epoxy and thin sectioned to a thickness of approximately 80–100 nm.

X-ray diffraction (*XRD*). The identification of the TiO_2 crystallographic phase anatase was carried out by means of an X'Pert diffractometer (Philips, Delft, The Netherlands). The Kα line of Cu (1.5409 Å) radiation was used as reference.

X-ray photoelectron spectroscopy (*XPS*). An AXIS NOVA photoelectron spectrometer (Kratos Analytical, Manchester, UK) provided with monochromatic AlK_a ($h\nu = 1486.6$ eV) was used to determine the atomic surface concentration of some of the elements on the PES–TiO_2 samples. The carbon C1 s line at 284.6 eV was used as a reference to correct the charging effect. The surface atomic concentration was determined from peak areas using known sensitivity factors for each element [23]. The spectrum background was subtracted according to Shirley [38]. The XPS spectral peaks of TiO_2 were deconvoluted by way of a CasaXPS-Vision 2 (Kratos Analytical).

Acknowledgements. We thank EPFL-CIME for their help with the electron microscopy experiments and the COST Actions MP1101 and 1106 for interactive discussions during the course of this study.

Funding statement. We thank the EPFL and Swiss National Science Foundation (SNF) Project (200021-143283/1) for financial support of this work.

References

1. Fujishima A, Zhang X, Tryk D. 2008 TiO_2 photocatalysis and related phenomena. *Surf. Sci. Rep.* **63**, 515–582. (doi:10.1016/j.surfrep.2008.10.001)
2. Page K, Wilson M, Parkin PI. 2009 Antimicrobial surfaces and their potential in reducing the incidence of hospital acquired infections. *J. Mater. Chem.* **19**, 3819–3831. (doi:10.1039/b818698g)
3. Daoud W (ed.). 2013 *Self-cleaning materials and surfaces*. Cambridge, UK: Woodhead Publishing Co.
4. Mills A, Lee S. 2002 A web-based overview of semiconductor photochemistry-based current commercial applications. *J. Photochem. Photobiol. A* **152**, 233–247. (doi:10.1016/S1010-6030(02)00243-5)
5. Dunlop PSM, Ciavola M, Rizzo L, Byrne J-A. 2011 Inactivation and injury assessment of *Escherichia coli* during solar and photocatalytic disinfection in LDPE bags. *Chemosphere* **85**, 1160–1166. (doi:10.1016/j.chemosphere.2011.09.006)
6. Rtimi S, Sanjines R, Andrzejczuk M, Pulgarin C, Kulik A, Kiwi J. 2014 Innovative transparent non-scattering TiO_2 bactericide films inducing increased *E. coli* cell fluidity. *Surf. Coat. Technol.* **254**, 333–343. (doi:10.1016/j.surfcoat.2014.06.035)
7. Pulgarin C, Kiwi J, Nadtochenko V. 2012 Mechanism of the photocatalytic destruction of bacteria by TiO_2 films leading to cell-wall damages and bacterial lysis. *Appl. Catal. B* **128**, 179–183. (doi:10.1016/j.apcatb.2012.01.036)
8. Rtimi S, Pulgarin C, Sanjines R, Kiwi J. 2015 Kinetics and mechanism for transparent polyethylene-TiO_2 films mediated self-cleaning leading to MB-dye discoloration under sunlight irradiation. *Appl. Catal. B* **162**, 236–244. (doi:10.1016/j.apcatb.2014.05.039)
9. Kramer A, Schwebke I, Kampf G. 2006 How long do nosocomial pathogens persist on inanimate surfaces? A systematic review. *BMC Infect. Dis.* **6**, 130–138. (doi:10.1186/1471-2334-6-130)
10. Dancer J. 2009 The role of environmental cleaning in the control of hospital-acquired infection. *J. Hosp. Infect.* **73**, 378–385. (doi:10.1016/j.jhin.2009.03.030)
11. Chan C, Ko T, Hiroaka H. 1996 Polymer surface modification by plasmas and photons. *Surf. Sci. Rep.* **24**, 1–54. (doi:10.1016/0167-5729(96)80003-3)
12. Bozzi A, Yuranova T, Kiwi J. 2005 Self-cleaning of wool-polyamide and polyester textiles by TiO_2-rutile modification under daylight irradiation at ambient temperature. *J. Photochem. Photobiol. A.* **172**, 27–33. (doi:10.1016/j.jphotochem.2004.11.010)
13. Zhang L, Dillert R, Bahnemann D, Vormoor M. 2012 Photo-induced hydrophilicity and self-cleaning: models and reality. *Energy Environ. Sci.* **5**, 7491–7507. (doi:10.1039/C2EE03390A)
14. Kiwi J, Nadtochenko V. 2004 New evidence for TiO_2 photocatalysis during bilayer lipid peroxidation. *J. Phys. Chem. B* **108**, 17 675–17 684. (doi:10.1021/jp048281a)
15. Amezaga-Madrid P, Sylveyra-Morales R, Cordoba-Fierro L, Nevarez-Moorillon G, Miki-Yoshida M, Orrantiaborunda E, Solis F. 2003 TEM evidence of ultrastructural alteration of *Pseudonomas aeruginosa* by photoctalytic TiO_2 thin film. *J. Photochem. Photobiol. B* **44**, 45–50. (doi:10.1016/S1011-1344(03)00054-X)
16. Foster A, Ditta I, Varghese S, Steele P. 2011 Photocatalytic disinfection using titanium dioxide: spectrum and mechanism of antimicrobial activity. *Appl. Microb. Biotech.* **90**, 1847–1868. (doi:10.1007/s00253-011-3213-7)
17. Baghriche O, Rtimi S, Pulgarin C, Roussel C, Kiwi J. 2013 RF-plasma pretreatment of surfaces leading to TiO_2 coatings with improved optical absorption and OH-radical production. *Appl. Cat. B* **130-131**, 65–72. (doi:10.1016/j.apcatb.2012.10.021)
18. Ishibashi K, Fujishima A, Watanabe T, Hashimoto K. 2000 Detection of active oxidative species in TiO_2 photocatalysis using the fluorescence technique. *Electrochem. Commun.* **2**, 207–210. (doi:10.1016/S1388-2481(00)00006-0)
19. Liu J, Roussel C, Lagger G, Tacchini P, Girault H. 2005 Antioxidant sensor based on DNA-modified electrodes. *Anal. Chem.* **77**, 7687–7694. (doi:10.1021/ac0509298)
20. Sakthivel S, Kisch H. 2003 Daylight photocatalysis of carbon modified TiO_2. *Angew. Chem. Int. Ed.* **42**, 4908–4913. (doi:10.1002/anie.200351577)
21. Park P, Kim W, Park H, Tachikawa T, Majima T, Choi W. 2009 Carbon-doped TiO_2 photocatalyst synthesized without using an external carbon precursor and the visible light activity. *Appl. Cat. B* **91**, 355–361. (doi:10.1016/j.apcatb.2009.06.001)
22. Mejía MJ, Marín M, Restrepo G, Pulgarín C, Mielczarski E, Mielczarski J, Arroyo A, Lavanchy J-A, Kiwi J. 2009 Self-cleaning TiO_2 cotton pretreated by RF-plasma and UV-C-light (185 nm) in vacuum and also under atmospheric pressure. *Appl. Catal. B* **91**, 481–488. (doi:10.1016/j.apcatb.2009.06.017)
23. Wagner D, Riggs M, Davis E, Müllenberg G (eds). 1979 *Handbook of X-ray photoelectron spectroscopy*. Eden Prairie, MN: Perkin-Elmer Corporation Physical Electronics Division.
24. Dhananjeyan M, Kiwi J, Thampi R. 2000 Photocatalytic performance of TiO_2 and Fe_2O_3 immobilized on derivatized polymer films for mineralisation of pollutants. *Chem. Commun.* **2000**, 1443–1444. (doi:10.1039/B003108I)
25. Castro C, Sanjines C, Pulgarin C, Osorio P, Giraldo S, Kiwi J. 2010 Structure–reactivity relations for DC-magnetron sputtered Cu-layers during *E. coli* inactivation in the dark and under light. *J. Photochem. Photobiol. A.* **216**, 295–302. (doi:10.1016/j.jphotochem.2010.06.030)
26. Rtimi S, Pulgarin C, Sanjines R, Kiwi J. 2013 Innovative semi-transparent nanocomposite films presenting photo-switchable behavior and leading to a reduction of the risk of infection under sunlight. *RSC Adv.* **3**, 16 345–16 349. (doi:10.1039/C3RA42762E)
27. Rtimi S, Baghriche O, Sanjines R, Pulgarin C, Ben-Simon MJ, Lavanchy J-C, Houas H, Kiwi J. 2012 Photocatalysis/catalysis by TiN/TiN-Ag surfaces efficient in bacterial inactivation under visible light. *Appl. Catal. B* **123–124**, 306–315. (doi:10.1016/j.apcatb.2012.04.047)

28. Jayachandran Y, Narayandass S. 2010 The effect of the thickness of Ti-nitride coatings on bacterial adhesion. *Trends Biomater. Artif. Org.* **24**, 90–93.
29. Hashimoto K, Irie H, Fujishima A. 2005 TiO_2 photocatalysis: an overview and future prospects. *AAPPS Bull.* **17**, 12–28. (doi:10.1143/JJAP.44.8269)
30. Sakai N, Fujishima A, Watanabe T, Hashimoto K. 2001 Enhancement of the photoinduced hydrophilic conversion rate of TiO_2 film electrode surfaces by anodic polarization. *J. Phys. Chem. B* **105**, 3023–3026. (doi:10.1021/jp003212r)
31. Pigeot-Rémy S, Simonet F, Errazuriz-Cerda E, Lazzaroni J, Atlan D, Guillard C. 2011 Photocatalysis and disinfection of water: identification of potential bacterial targets. *Appl. Cat. B* **104**, 390–398. (doi:10.1016/j.apcatb.2011.03.001)
32. Rio L, Kusiak E, Kiwi J, Pulgarin C, Trampuz C, Bizzini A. 2012 Comparative methods to evaluate the bactericidal activity of copper-sputtered surfaces against methicillin-resistant *Staphylococcus aureus*. *Appl. Environ. Microb.* **78**, 8176–8182. (doi:10.1128/AEM.02266-12)
33. Poole R, Kumar I, Salmonl I, Chance B. 1983 The 650 and chromophore in *Escherichia coli* is 'oxy-' or oxygenated compound, not the oxidized form of cytochrome oxidase: an hypothesis. *J. Gen. Microb.* **129**, 1335–1344.
34. Loosdrecht van L, Lyklema M, Norde W, Schraa G, Zender A. 1987 The role of bacterial cell wall hydrophobicity in adhesion. *Appl. Environ. Microb.* **53**, 1893–1990.
35. Xu L, Wellia D, Amal R, Liao W, Loo J, Tan T. 2010 Fabrication of highly ordered TiO_2 nanorod/nanotube adjacent arrays for photoelectrochemical applications. *Langmuir* **2**, 1122–1128.
36. Gunawan C, Teoh W, Marquis P, Lifla J, Amal R. 2009 Reversible antimicrobial photo-switching in nanosilver. *Small* **5**, 341–344. (doi:10.1002/smll.200801202)
37. Nogier N, Delamar M, Grätzel M, Thampi K, Albers P, Kiwi J. 1994 X-ray photoelectron spectroscopy of V_2O_5/TiO_2 catalysts. *Catalysis Today* **20**, 109–123. (doi:10.1016/0920-5861(94)85020-8)
38. Shirley D. 1972 Corrections of electrostatic charged species in XPS-spectroscopy. *Phys. Rev.* **B5**, 4709–4716. (doi:10.1103/PhysRevB.5.4709)
39. Harmer A, Farneth W, Sun Q. 1996 High surface Nafion resin/silica nanocomposites. *J. Am. Chem. Soc.* **118**, 7708–7715. (doi:10.1021/ja9541950)
40. Kiwi J, Morrison C. 1984 Heterogeneous photocatalysis. Dynamics of charge transfer in lithium-doped anatase-based catalyst powders with enhanced water photocleavage under ultraviolet irradiation. *J. Phys. Chem.* **88**, 6146–6152. (doi:10.1021/j150669a018)
41. Nesic J, Rtimi S, Laub D, Roglic MG, Pulgarin C, Kiwi J. In press. New evidence for TiO_2 uniform surfaces leading to complete bacterial reduction in the dark: critical issues. *Coll. Surf. Biointerf.* (doi:10.1016/j.colsurfb.2014.09.060)
42. Caballero L, Whitehead A, Allen S, Verran S. 2009 Inactivation of *E. coli* on immobilized TiO_2 using fluorescent light. *J. Photochem. Photobiol. A.* **202**, 92–98. (doi:10.1016/j.jphotochem.2008.11.005)
43. Sunada K, Watanabe K, Hashimoto K. 2003 Studies on the photokilling of bacteria on TiO_2 thin film. *J. Photochem. Photobiol. A* **156**, 227–233. (doi:10.1016/S1010-6030(02)00434-3)
44. Rtimi S, Baghriche O, Pulgarin C, Lavanchy J-V, Kiwi J. 2013 Growth of TiO_2/Cu by HiPIMS for accelerated bacterial loss of viability. *Surf. Coat Techniol.* **232**, 804–813. (doi:10.1016/j.surfcoat.2013.06.102)